

Mechanical properties analysis of burnished brass

Mayas Mohammad Al-mahasne¹ 

¹ Mechanical Engineering Department, Tafila Technical University, Tafila, Jordan
E-mail: mahasnem@yahoo.com

ABSTRACT

Brass alloy consists of copper and zinc. It is used as an industrial material because of its hardness and workability, high corrosion resistance, magnetism and good forging ability. This paper evaluates the mechanical properties of brass alloy subjected to cold working which caused plastic straining of the surface of brass specimen resulting from burnishing forces. Forces have a significant role in a burnished surface of brass sample which squeeze it against the samples making plastic twisting of the specimen surface. Burnishing results under variable forces are investigated. The best results of surface roughness have the forces rate of more than 100 N. with a feed rate (0.07 mm/rev).

Keywords: yellow brass, mechanical properties, burnishing, cold working, hardness, bending and torsion.

INTRODUCTION

Burnishing is to impose a force on the surface of specimen to make plastic deformation using a hardened tool [1]. This plastic deformation/ cold working is expected to change the properties of the burnished specimen [2]. Researchers have studied the effect of different burnishing tools on the properties of the specimen [3–6], ball burnishing [7,8], roller burnishing [9, 10] and diamond burnishing tool [11–13]. Recently the burnishing process showed increasing interest for researchers, development of burnishing process for better surface finish was analyzed [14]. The advances in burnishing technologies were investigated in the last few years [15]. Varpe, and Tajane, in (2025) performed an overview of burnishing process as a Surface improvement technique [16]. Brass has many engineering applications, especially for resisting corrosion where low friction is required, such as valves, gears, pipes and various precision components. Because of ease manufacturing and corrosion resistance, brass also became the standard allow from which all precision instruments were made. The performance of the mechanical properties of the machined component (fatigue, bearing capacity, wear) depend largely on the component surface topography and/or hardness, stress and induced

strain. More than 55% of the input energy is demolished in kinetic friction [17, 18]. Low roughness $< 0.1 \mu\text{m}$ gives good esthetic appearance, easy mold detachment, higher corrosion resistance (CR), and good fatigue strength (FS). Recently, high attention was given to the post-machining metal finishing operations such as burnishing. Burnishing improves the surface conditions by cold working on surface layers [19]. In a cold-forming process, burnishing is crucial because it fills the depression by pushing the metal close to a machined surface away from protrusions. A comprehensive classification of burnishing tools and their application has been reviewed by Raza and Kumar [20]. Literature inspection shows that many researchers have worked on the burnishing process, they conducted many improvements on the properties of the materials [21, 22], for example better friction resistance and hardness [23–25], surface finishing [26, 27] and permanent compression stress reaching high values [28]. Surface finish is affected by burnishing force (BF), feed rate (FR), roller material (RM), number of passes, specimen material, in addition to lubrication [29, 30].

It is clear from literature the burnishing process may be used to improve the surface properties and mechanical properties of a material and as brass is one of the important materials used in engineering,

this paper will study the effect roller burnishing (RB) process, BF on the mechanical properties of the material (tensile, compression and torsion stresses in addition to surface hardness) to give better surface integrity for yellow Brass.

MATERIALS AND METHODS

Materials

To prepare the specimens for testing various burnishing forces a lathe machine with roller head burnishing tool were used. Figure 1 shows the burnishing process of a brass specimen on a lathe machine. Burnishing process requires the use of a dial gauge to measure the pressing force, a roller head, a pure brass test specimen all with the lathe machine. Different brass specimens were burnished under different pressing forces (0, 60, 90, 120 and 140 N), with tool feed rate 0.07 mm/rev.

The chemical composition of the used yellow Brass is indicated in Table 1. While the physical parameters are indicated in Table 2.

Methodology

Each test was performed with four specimens to assure the results for (tensile, compression, torsion and hardness). A universal testing machine (UTM), also known as a tensile tester or universal tensile tester, is a universal device used to test the mechanical properties of the material under tension, compression, bending and other forces.

Table 1. Chemical composition of the used Brass

Copper	65%
Zinc	34%
Lead	1%

Table 2. Physical parameters of the used Brass

Specific gravity	8.53
Specific heat	0.377 J/kg. K
Thermal conductivity	121 W/m K
Thermal expansion coefficient	19.9 $\mu\text{m}/\text{m} \cdot ^\circ\text{C}$
Modulus of elasticity	110 GPa
Shear modulus	41 GPa
Ultimate tensile strength	393–455 MPa
Yield tensile strength	365–434 MPa
Hardness	49–53 VHR



Figure 1. Burnishing tool and lath machine

It plays a critical role in determining the strength and durability of materials such as metal and metal alloys. The strain of a workpiece indicates quantitatively the deformation of a body. It can be measured with extensometers and/or strain gauges. The uniaxial strain is expressed by:

$$e = \frac{l_f - l_o}{l_o} \quad (1)$$

where: l_f – deformed specimen length, l_o – undeformed specimen length.

If a specimen is stretched such as $l_f = 2l_o$ the engineering tensile strain equal to 100%. If a specimen is compressed to the amount of $l_f = 0$, the engineering compressive strain equals 100% which has no engineering meaning Equation 1.

As the stresses of purely elastic deformation (ED) are defined using the material final configuration. Due to irreversibility in the deformation, a plastic analysis must be followed along the final path reached. To do so, the total deformation is subdivided into infinitesimal increments. For the uniaxial case, with dL – the gauge length incremental change, L – the increment starting gauge length. Then, the strain increment is:

$$d\varepsilon = \frac{dl}{l} \quad (2)$$

the total strain from l_o to l_f

$$\varepsilon = \int_0^\varepsilon d\varepsilon = \int_{l_o}^{l_f} \frac{dl}{l} = \ln \frac{l_f}{l_o} \quad (3)$$

Which defines the true strain. So, if a sample is compressed to zero thickness, Equation 3 becomes:

$$\varepsilon_{l_f} = \lim_{l_f \rightarrow 0} \left(\ln \frac{l_f}{l_o} \right) = -\infty \quad (4)$$

Which is a more realistic than 100% compressive strain which was given by Equation 1. The relation between true and engineering strain is:

$$\varepsilon = \ln(1 + e) \quad (5)$$

If a body with original cross-sectional area A_o (mm^2) is subjected to a load F (N), the stress, s for uniform deformation can be defined as:

$$s = \frac{F}{A_o} \text{ (MPa)} \quad (6)$$

which refers to the undeformed configuration, such stress is called engineering stress. For large cross-sectional area reduction this definition becomes inappropriate. Such definition fails to predict strain hardening as it uses constant initial area A_o . The instantaneous cross-sectional area (CSA) A must be used to give more realistic stress:

$$\sigma = \frac{F}{A} \quad (7)$$

This definition of stress σ uses the instantaneous CSA and named true stress. As the volume of the deformed specimen is conserved, i.e.:

$$A_o L_o = A_f L_f \quad (8)$$

The true stress can be related to engineering stress by:

$$\sigma = s(1 + e) \quad (9)$$

Only small deformations use engineering stress-strain diagrams, where true stress-strain coincides with engineering stress strain diagram within Hook's law. For large strain, say greater than 1%, the true stress-strain should always be used. Equation 6 is used for uniform deformation only. In non-uniform deformation, stress is

$$\sigma = \lim_{\Delta A \rightarrow 0} \left(\frac{\Delta F}{\Delta A} \right) \quad (10)$$

These equations from Equation 1 to Equation 10 are used to analyze the experimental results of yellow brass specimens. It is difficult to measure ΔA in Equation 10, then we can use the specimen

lengths instead of using CSA. This suggests that only when deformation is homogeneous can stress s be directly determined by measuring the force and the associated cross-sectional area. Only the average stress can be measured once the deformation stops being uniform; the experimental determination of the stress distribution is impossible. This is the primary cause of the issues that arise while attempting to determine actual tension following necking.

Tensile test

The tensile test done is a standard method used to measure the behavior of the materials when they are pulled apart, it can give information about the material properties and show how strong brass is. Common standards include ASTM E8 was used to determine the tensile properties of metals, these standards guide testing method. These experiments enhance our knowledge in practical problems. All samples were tested with Instron machine for tensile and compression strength.

Combined bending and torsion

WP130 test unit Figure 2 is used to test experimentally the material strength of various specimens. Principal stresses can be used to measure the stress of a material by subjecting the specimen to a component with combined shearing and direct loads. The equation of the combined bending and torsion stress is given by:

$$\sigma_c = 2 \tau_{max} = \sqrt{(\sigma_x - \sigma_y)^2 + 4\tau^2} \quad (11)$$

where: σ_c is the combined stress, σ_x max. direct bending stress, σ_y is zero in this case, τ torsion stress.

The maximum bending stress in the edge fiber is calculated from the bending moment and the geometric moment of inertia:

$$\sigma_x = \frac{M_b d}{I_b} \quad (12)$$

The maximum shear stress in the edge fiber is calculated from the torsion moment as:

$$\tau = \frac{M_t d}{I_t} \quad (13)$$

The geometric moments of inertia for a circular cross-section are:

$$I_b = \frac{d^4 \pi}{64}, \quad I_t = \frac{d^4 \pi}{32} = 2I_b \quad (14)$$

The external bending moment M_b and the torque M_t can be calculated with the angle position

φ of the point of contact and the load weight F to (see Figure 3):

$$M_b = F r \cos\varphi, M_t = F r \sin\varphi \quad (15)$$

If the bending moment and the torque are used the following results:

$$\sigma_c^2 = \frac{d^2}{4} \left[\left(\frac{F r \cos\varphi}{I_b} \right)^2 + 4 \left(\frac{F r \sin\varphi}{2I_b} \right)^2 \right] \quad (16)$$

$$\sigma_c = \frac{F r d}{2I_b} \sqrt{\cos^2 \varphi + \sin^2 \varphi} \quad (17)$$

The $\cos^2 \varphi + \sin^2 \varphi$ can be combined to 1.

RESULTS

Figure 4 shows the relation between normal stress and normal strain for various burnishing forces (0, 60, 90, 120 and 140 N). Fracture and yield strengths are improved for specimens after burnishing which can play role in industrial

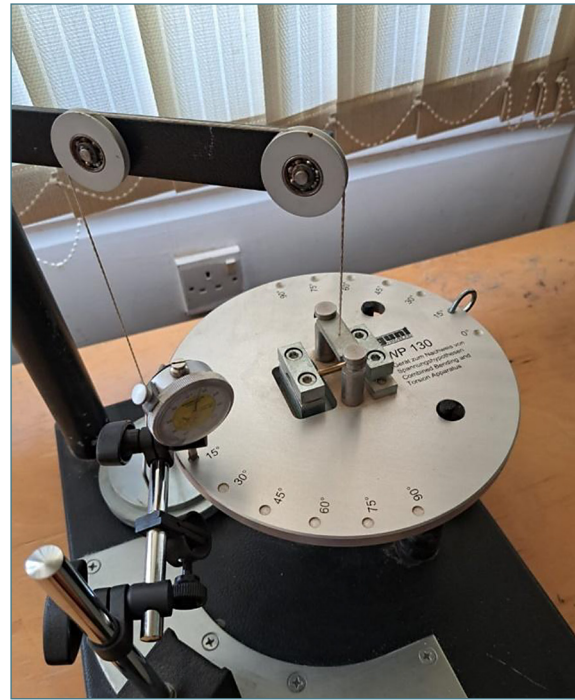


Figure 2. Bending and torsion apparatus WP 130

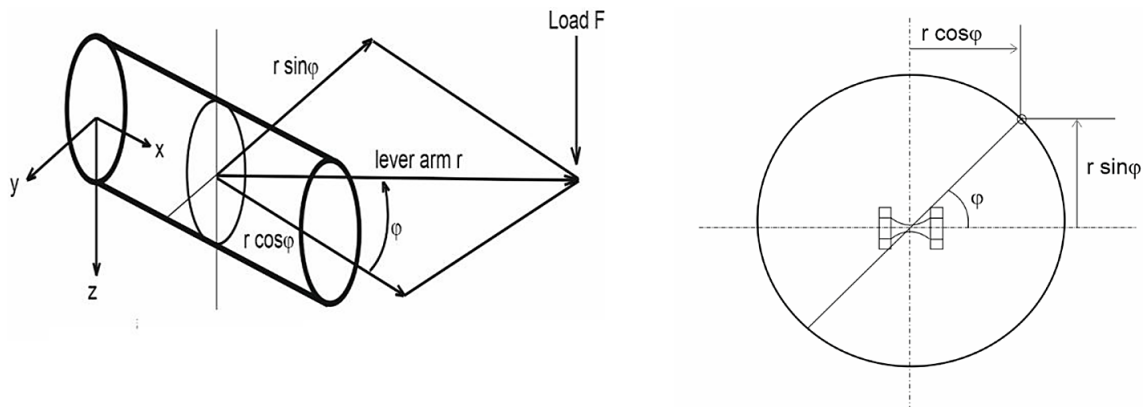


Figure 3. Schematic of bending and torsion loading of specimen

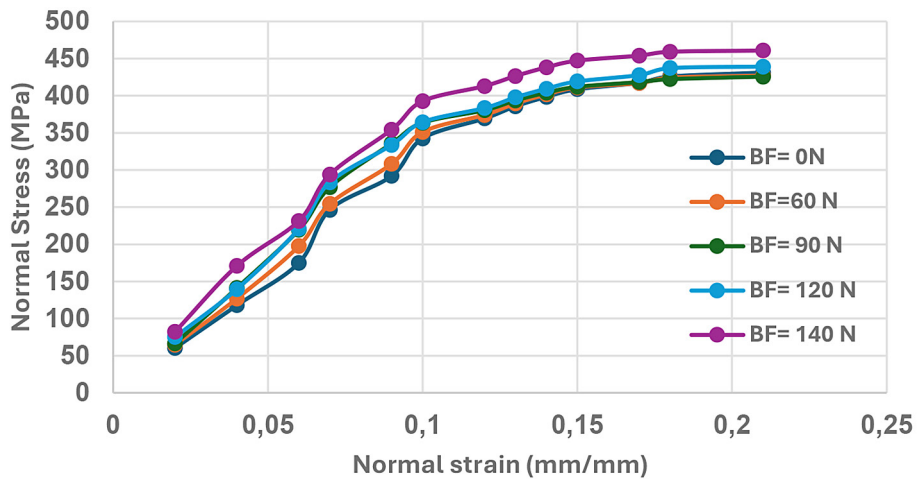


Figure 4. Normal stress–strain diagram of yellow brass



Figure 5. The Instron tensile machine with the fractured tool

applications. It can be seen from Figure 4 that the higher values of normal stresses are the values where the BF=140 N, which gives the best results, the results of normal stresses of specimens which have BF= 90, 120 N have also good results.

Instron tensile machine and real fractured specimens are shown in Figure 5. Using Equations 1, 3, and 5 true and engineering strain relation were calculated from the experimental data. Figure 6 shows the true strain-engineering strain relation. Figure 6 indicates that by increasing engineering strain the true strain also increased by the linear relation, but the values of engineering strain are higher than the true strain due to

engineering behavior of b.rass. Figure 7 illustrates the true stress true strain curves for various burnishing forces (0, 60, 90, 120 and 140 N).

As shown in Figure 7 the best result was achieved for 120 and 140 N, which means that these brass specimens exhibit high stress with 120 N and 140 N burnishing forces.

Figure 8 points out the relation between tensile force and engineering strain of yellow brass specimens which were subjected to variable BF. Figure 8 reveals that the specimens with BF=140 N have better results, especially at $\epsilon \geq 0.08$. The specimens with BF = 120 N have good results at low values, and high values of engineering strain.

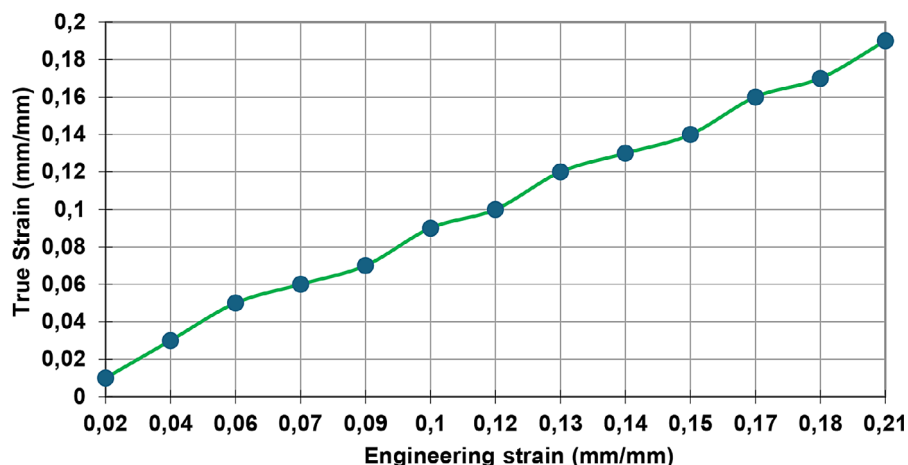


Figure 6. True strain-engineering strain diagram of yellow brass

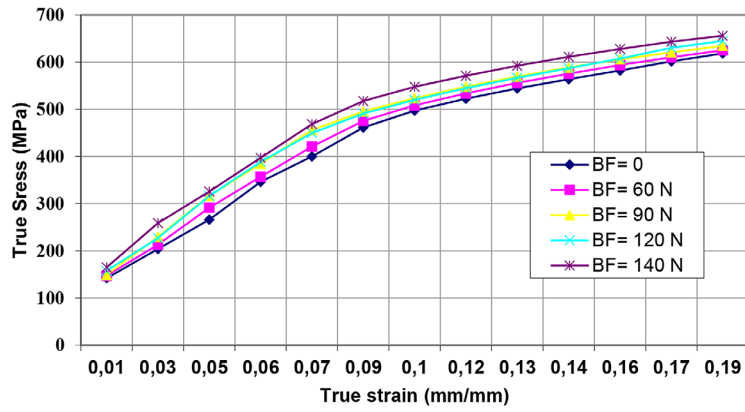


Figure 7. True stress–strain diagram of yellow brass

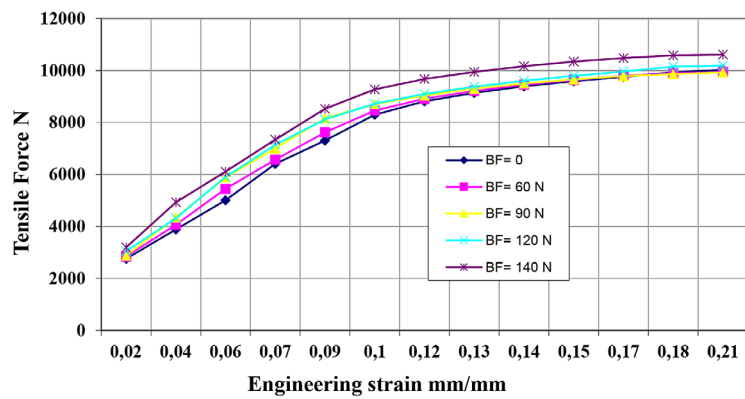


Figure 8. Tensile force– engineering strain diagram of yellow brass

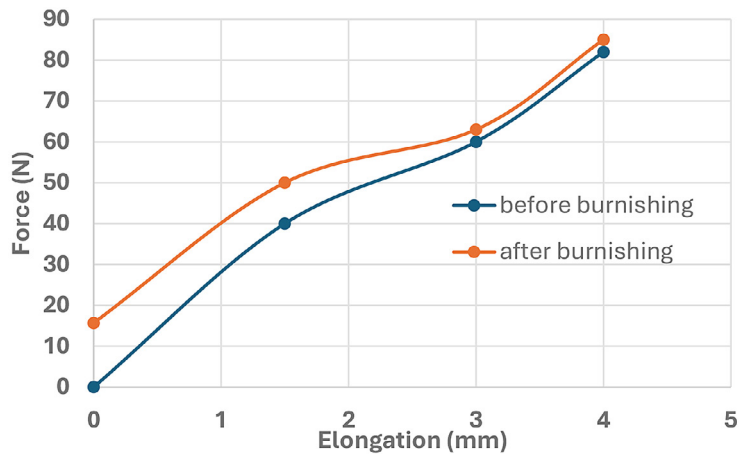


Figure 9. Force– elongation of yellow brass before and after burnishing

The specimen of BF = 90 N gives bad results at $\epsilon \geq 0.12$. Figure 9 illustrates the force versus elongation behavior before and after burnishing. It is clear from the figure that the unburnished specimen starts elongation directly from zero, where the burnished specimen begins elongation from 17 N which indicates the positive impact of burnishing process on the specimen mechanical

properties. This effect proceeds all over the various burnishing forces. Also, as the applied force increases the effect of burnishing decreases on the specimen. The percentage decreasing of elongation of specimens under the burnishing forces shown in Table 3. As shown in Table 3. the burnishing force variation decreases with increasing in elongation, and at high values of elongation the

variation of force is negligible. While at low values the effect of elongation the BF effect is clear.

Its shown in Table 4. That the improvement of VH decreases as BF increases due to cold working of the specimen.

Table 3. Burnishing force versus specimen elongation percentage

Elongation (mm)	BF variation (N)
1	13
2	7
3	4
4	4

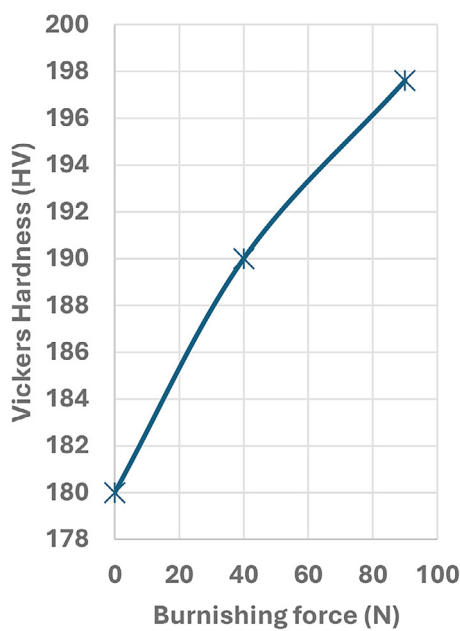


Figure 10. Vickers Hardness versus BF of yellow Brass before and after burnishing

Figure 10 illustrates the impact of BF on the surface hardness of the yellow Brass. The Vickers hardness of yellow Brass was tested for unburnished specimen and specimens with 40 N and 90 N burnishing forces. It is obvious in the figure that the increase in BF increases the surface hardness significantly. This result is important in the applications encounter surface erosion. As shown from Figure 11 by increasing the BF the specimen exhibits a high UTS. The percentage elongation of UTS for specimens shown in Table 5.

Figure 12 indicates that the reduction in area decreases with an increase of BF. As is clear from the figure the reduction in area remains constant at high burnishing forces, and that is due to the condensation of material particles layers with increasing BF.

Figure 13 shows the reduction in mean roughness as BF increases, because the surface of the specimen becomes more polished. In Figure 14.

Table 4. Burnishing force-VH %

BF (N)	VH (%)
40	25
60	15
90	13

Table 5. Burnishing force-UST increment %

BF (N)	UTS increment (%)
60	10.8
90	33
120	34
140	54

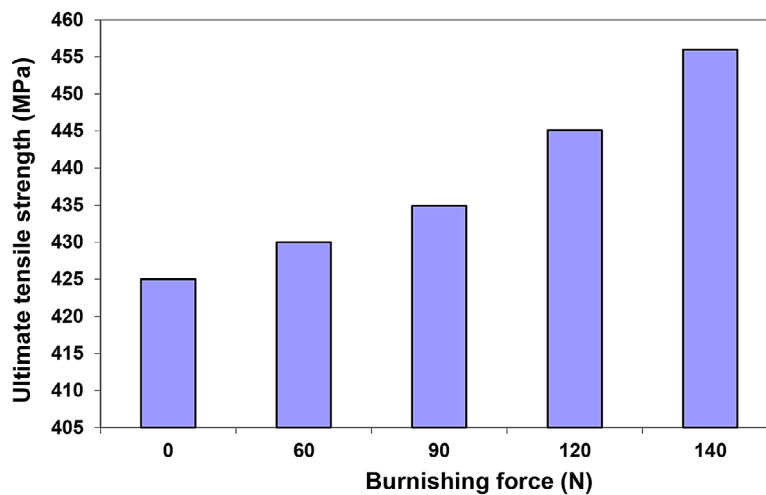


Figure 11. Burnishing force versus ultimate tensile strength

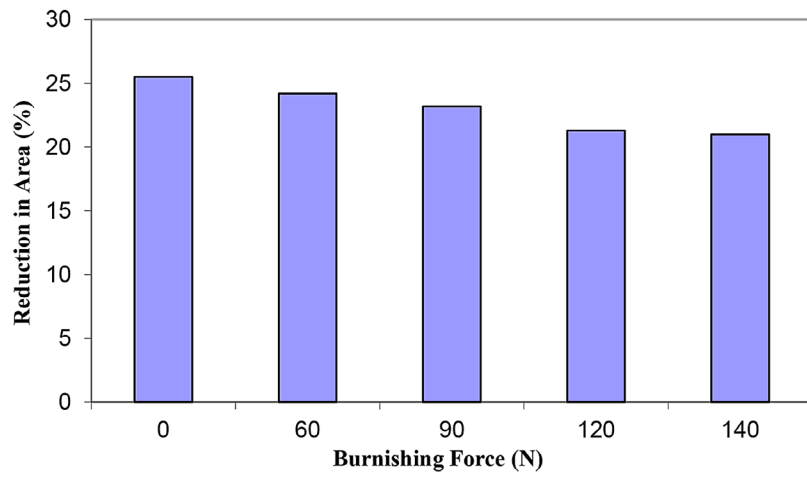


Figure 12. Burnishing force versus reduction in area of yellow brass before and after burnishing

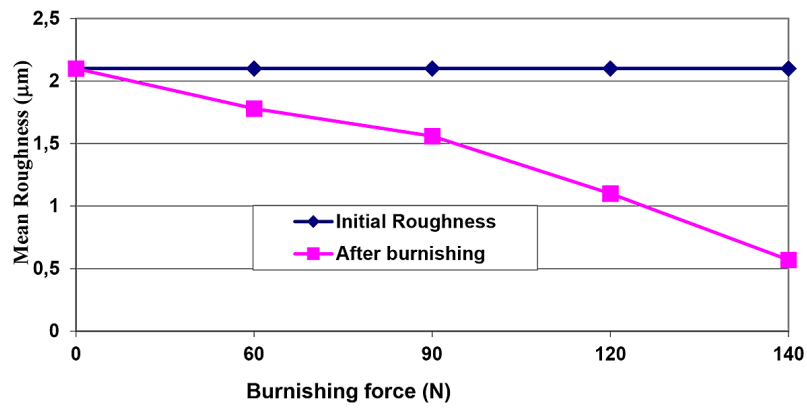


Figure 13. Burnishing force versus mean roughness

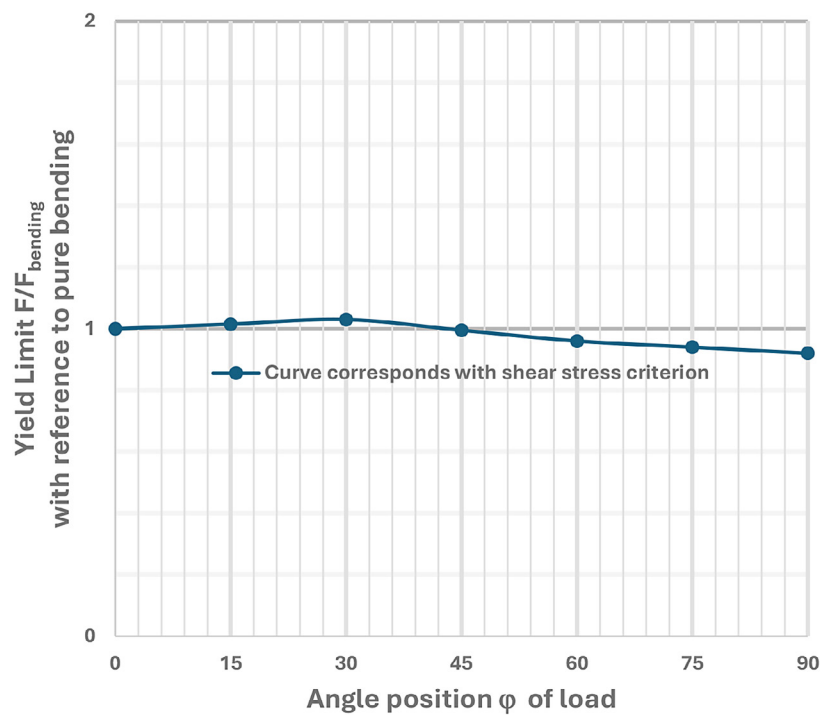


Figure 14. Position angle φ of load versus yield limit (reference to pure bending)

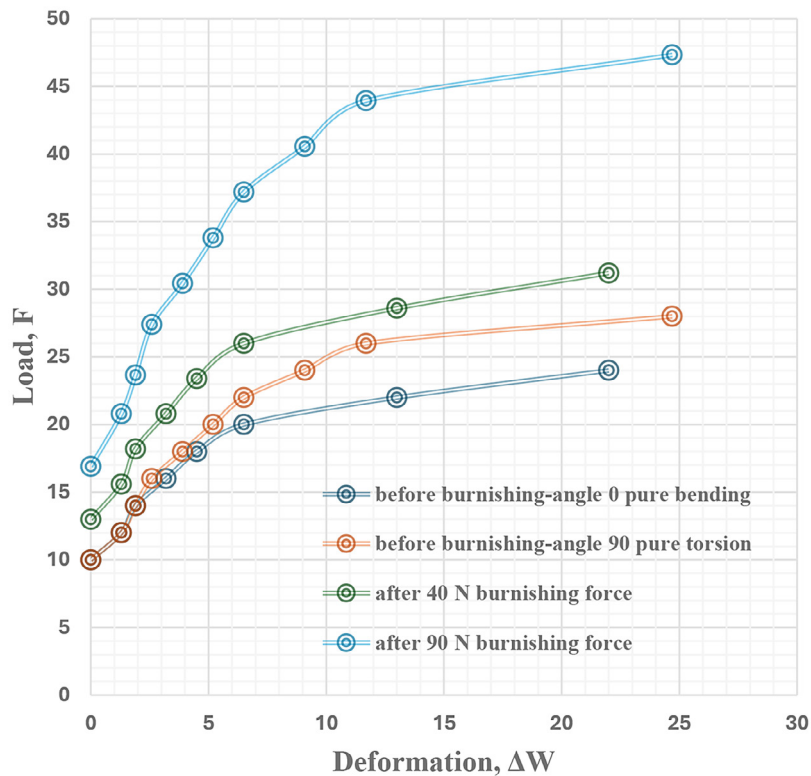


Figure 15. Load deformation diagram for different positions of specimen before and after burnishing

the dependency of yield limit in type of load of a brass spaceman has been determined for all angle positions, the mean of both runs is determined and referenced to the pure bending value (angle 0°), this results in horizontal curve shown with shear stress criteria. The yield limit is determined by graphing the load over remaining deformation (ΔW) and shown in Figure 15, at point 10 it clearly shows the increasing of strength as a result of strain hardening.

CONCLUSIONS

The effect of BF on the yellow brass mechanical properties was studied. Yellow brass tensile, compression, bending and torsion properties were tested, results were analyzed, and the preferred burnishing force was determined in the sample with 140 N BF. According to tensile test results this sample exhibits the best mechanical properties (nonductile behavior under higher load).

As results of the experimental investigations, the following can be concluded:

1. The surface roughness decreases from 2.1 μm to 0.57 μm at high values of BF (120, and 140 N).
2. The reduction in the area decreases from 25.5% to 21% by increasing BF.

3. The minimum tensile strength of specimen after burnishing increased from 425 MPa to 456 MPa.
4. The Vickers' hardness percentage increased from 180 to 197 HV by increasing BF.

REFERENCES

1. Vaishya, R. O., Sharma, V., Mishra, V., Gupta, A., Dhanda, M., Walia, R. S.,... & Burduhos-Nergis, D. P. Mathematical modeling and experimental validation of surface roughness in ball burnishing process. *Coatings*, 2022; 12(10), 1506. <https://doi.org/10.3390/coatings12101506>
2. Varga, G., Ferencsik, V. Investigation of the effect of surface burnishing on stress condition and hardening phenomena. *Tehnički vjesnik*, 2022; 29(4), 1247–1253] <https://doi.org/10.17559/TV-20211110171854>
3. Raza, A., Kumar, S. A critical review of tool design in burnishing process. *Tribology International*, 2022; 174, 107717; <https://doi.org/10.1016/j.triboint.2022.107717>
4. Mahajan, D., Tajane, R. A review on ball burnishing process. *International Journal of Scientific and Research Publications*, 2013; 3(4), 1–8.
5. Tadic, B., Todorovic, P. M., Luzanin, O., Miljanic, D., Jeremic, B. M., Bogdanovic, B., Vukelic, D. Using specially designed high-stiffness burnishing tool to achieve high-quality surface finish. The

- International Journal of Advanced Manufacturing Technology, 2013; 67, 601–611. <https://doi.org/10.1007/s00170-012-4508-2>
6. Shiou, F. J., Huang, S. J., Shih, A. J., Zhu, J., Yoshino, M. Fine surface finish of a hardened stainless steel using a new burnishing tool. *Procedia manufacturing*, 2017; 10, 208–217. <https://doi.org/10.1016/j.promfg.2017.07.048>
 7. Becerra-Becerra, E., Ojeda, C. A., Saldaña-Robles, A., Reveles-Arredondo, J. F., Barco-Burgos, J., Vidal-Lesso, A. A review of numerical simulation of ball burnishing process. *Finite Elements in Analysis and Design*, 2023; 218, 103926. <https://doi.org/10.1016/j.finel.2023.103926>
 8. Kapoor, M., Jawalkar, C. S. A review on critical aspects of the burnishing process. *i-Manager's Journal on Material Science*, 2016; 3(4), 44. <https://doi.org/10.26634/jms.3.4.4827>
 9. Yen, Y. C., Sartkulvanich, P., Altan, T. Finite element modeling of roller burnishing process. *CIRP annals*, 2005; 54(1), 237–240. [https://doi.org/10.1016/S0007-8506\(07\)60092-4](https://doi.org/10.1016/S0007-8506(07)60092-4)
 10. Nguyen, T. T., Le, X. B. Optimization of interior roller burnishing process for improving surface quality. *Materials and Manufacturing Processes*, 2018; 33(11), 1233–1241. <https://doi.org/10.1080/10426914.2018.1453159>
 11. Okada, M., Shinya, M., Matsubara, H., Kozuka, H., Tachiya, H., Asakawa, N., Otsu, M. Development and characterization of diamond tip burnishing with a rotary tool. *Journal of Materials Processing Technology*, 2017; 244, 106–115. <https://doi.org/10.1016/j.jmatprotec.2017.01.020>
 12. Duncheva, G. V., Maximov, J. T., Anchev, A. P., Dunchev, V. P., Argirov, Y. B. Multi-objective optimization of the internal diamond burnishing process. *Materials and Manufacturing Processes*, 2022; 37(4), 428–436. <https://doi.org/10.1080/10426914.2021.1981937>
 13. Nguyen, T. T., Van, A. L. Machining and optimization of the external diamond burnishing operation. *Materials and Manufacturing Processes*, 2023; 38(10), 1276–1290. <https://doi.org/10.1080/10426914.2022.2072880>
 14. Jagadeesh, G. V., Gangi Setti, S. A review on latest trends in ball and roller burnishing processes for enhancing surface finish. *Advances in Materials and Processing Technologies*, 2022; 8(4), 4499–4523. <https://doi.org/10.1080/2374068X.2022.2077534>
 15. Slavov, S. D., Dimitrov, D. M., Konsulova-Bakalova, M. I. Advances in burnishing technology. In *Advanced Machining and Finishing 2021*; 481–525. Elsevier. <https://doi.org/10.1016/B978-0-12-817452-4.00002-6>
 16. Varpe, N. J., Tajane, R. Overview of burnishing process as a surface improvement technique. *Manufacturing Strategies and Systems*, 2025; 234–266. <https://doi.org/10.1201/9781032725086-16>
 17. Abdullah, R., Beithou, N. Burnishing effects on friction stir welding of Al-Alloy 7075 T6. *Global Journal of Researches in Engineering: A Mechanical and Mechanics Engineering*, 2014; 14(3), 12–19.
 18. Hao, L., Pagani, R., Beschi, M., Legnani, G. Dynamic and friction parameters of an industrial robot: Identification, comparison and repetitiveness analysis. *Robotics*, 2021; 10(1), 49. <https://doi.org/10.3390/robotics10010049>
 19. Babu, P. R., Ankamma, K., Prasad, T. S., Raju, A. V. S., Prasad, N. E. Optimization of burnishing parameters by DOE and surface roughness, microstructure and micro hardness characteristics of AA6061 aluminium alloy in T6 condition. *International Journal of Engineering Research and Applications*, 2012; 2(2), 1139–1146.
 20. Raza, A., Kumar, S. A critical review of tool design in burnishing process. *Tribology International*, 2022; 174, 107717. <https://doi.org/10.1016/j.triboint.2022.107717>
 21. El-Axir, M. H., El-Khabeery, M. M. Influence of orthogonal burnishing parameters on surface characteristics for various materials. *Journal of Materials Processing Technology*, 2003; 132(1–3), 82–89. [https://doi.org/10.1016/S0924-0136\(02\)00269-8](https://doi.org/10.1016/S0924-0136(02)00269-8)
 22. Nguyen, T. T., Cao, L. H. Optimization of the burnishing process for energy responses and surface properties. *International Journal of Precision Engineering and Manufacturing*, 2020; 21(6), 1143–1152. <https://doi.org/10.1007/s12541-020-00326-8>
 23. Revankar, G. D., Shetty, R., Rao, S. S., Gaitonde, V. N. Wear resistance enhancement of titanium alloy (Ti–6Al–4V) by ball burnishing process. *Journal of Materials Research and Technology*, 2017; 6(1), 13–32. <https://doi.org/10.1016/j.jmrt.2016.03.007>
 24. Grudzień, J., Grochała, D., Grzejda, R., Kochmański, P. Testing the Effectiveness of Hybrid Milling and Surface Burnishing in Improving the Wear Resistance of Machine Parts Made of Structural Steel. *Lubricants*, 2024; 12(12), 458. <https://doi.org/10.3390/lubricants12120458>
 25. Attabi, S., Himour, A., Laouar, L., Motallebzadeh, A. Mechanical and wear behaviors of 316L stainless steel after ball burnishing treatment. *Journal of Materials Research and Technology*, 2021; 15, 3255–3267. <https://doi.org/10.1016/j.jmrt.2021.09.081>
 26. Cobanoglu, T., Ozturk, S. Effect of burnishing parameters on the surface quality and hardness. *Proceedings of the Institution of Mechanical Engineers, Part B: Journal of Engineering Manufacture*, 2015; 229(2), 286–294. <https://doi.org/10.1177/0954405414527962>
 27. Nguyen, T. T., Le, X. B. Optimization of interior

- roller burnishing process for improving surface quality. *Materials and Manufacturing Processes*, 2018; 33(11), 1233–1241. <https://doi.org/10.1080/10426914.2018.1453159>
28. Sartkulvanich, P., Altan, T., Jasso, F., Rodriguez, C. Finite element modeling of hard roller burnishing: an analysis on the effects of process parameters upon surface finish and residual stresses. 2007. <https://doi.org/10.1115/1.2738121>
29. Jagadeesh, G. V., Gangi Setti, S. A review on latest trends in ball and roller burnishing processes for enhancing surface finish. *Advances in Materials and Processing Technologies*, 2022; 8(4), 4499–4523. <https://doi.org/10.1080/2374068X.2022.2077534>
30. Cao, C., Zhu, J., Tanaka, T., Shiou, F. J., Sawada, S., Yoshioka, H. Ball burnishing of Mg alloy using a newly developed burnishing tool with on-machine force control. *International Journal of Automation Technology*, 2019; 13(5), 619–630. <https://doi.org/10.20965/ijat.2019.p0619>